

# Broadband and Giant Nonreciprocity in Subwavelength Plasmonic Structures

Mohamed Ismail Abdelrahman\* and Francesco Monticone†

Cornell University, School of Electrical and Computer Engineering, Ithaca, New York 14853, USA

We unveil a previously overlooked wave propagation regime in magnetized plasmonic (gyrotropic) materials with comparable plasma and cyclotron frequencies, which enables a giant and broadband (non-dispersive) non-reciprocal response. We show that this effect ultimately originates from the subtle implications of the principle of causality for gyrotropic plasmonic media, which allows the existence of a low-loss frequency window with anomalous non-monotonic dispersion for the extraordinary mode. This is in stark contrast with conventional non-gyrotropic passive materials, for which the frequency derivative of the permittivity dispersion function is always positive in low-loss regions. These findings pave the way for superior nonreciprocal components in terms of bandwidth of operation and compactness, with orders-of-magnitude reductions in size, in particular at THz frequencies and beyond. As a relevant example, we consider Indium Antimonide (InSb) to theoretically demonstrate a deeply subwavelength, broadband, THz isolator operating at room temperature and under moderate magnetic bias.

Breaking Lorentz reciprocity in electromagnetic systems enables a plethora of complex devices with rich functionalities to control wave propagation in anomalous ways, such as circulators, nonreciprocal phase shifters, asymmetric polarization converters, and isolators. Nonreciprocal effects can be accomplished using various techniques, for example, by exploiting the precession motion of spinning electrons or the cyclotron motion of free electrons in ferrites and plasma media, respectively, under a static magnetic field [1–3]. Alternatively, in recent years, magnetic-free techniques have been extensively investigated by leveraging other forms of bias that break time-reversal symmetry, as in artificially engineered metamaterials biased by linear/angular momentum [4, 5] or, more generally, in spatio-temporally modulated media [6–8]. Nonlinear effects have also been exploited to achieve nonreciprocity [9, 10], yet of a weaker form, and limited to applications in which the device is not simultaneously excited from both sides (dynamic nonreciprocity constraints [11]). We refer the interested reader to Ref. [12] for a comprehensive review of nonreciprocal effects and devices.

Within this context, achieving giant nonreciprocity in *broadband* and *compact* devices is an active area of research with several applications at microwaves, THz, and optical frequencies. Particularly appealing are emerging applications in the so-called “THz gap,” which extends from the high-end of the millimeter-wave band to the low-end of the far-infrared light band [13], such as ultra-broadband communications, advanced THz imaging, and THz microscopy and spectroscopy for material and device characterization [13–16]. For many of these applications across the electromagnetic spectrum, unidirectional transmission devices (isolators) are often crucial to protect electromagnetic sources and amplifiers from detrimental back reflections.

Attempts to realize broadband isolators rely on many different mechanisms, each with its own limitations. Examples include wavelength-insensitive isolators based on dispersion compensation using additional optical elements [17, 18], which are, however not suitable for integration in monolithic systems due to their bulkiness; broadband nonlinear effects using multiple resonators [19], which suffer from the fun-

damental limitations and constraints mentioned above; and time-modulated microwave/millimeter-wave circuits based on balanced delay lines with switches [20], which are, however, difficult to scale beyond the millimeter-wave range. Historically, the most common approach to realize broadband non-reciprocal devices at microwave frequencies has been to use ferrimagnetic materials (ferrites and magnetic garnets) under static magnetic bias, which naturally exhibit a dispersion-less broadband region of Faraday rotation [2, 21]. The operation of ferrite-based microwave isolators that rely on a strongly gyrotropic *permeability* tensor can be pushed up to a few hundreds of GHz using suitable materials [21], but their magnetic response tails off at THz frequencies as their permeability converges to that of free-space. Moreover, at even higher frequencies, most magneto-optical materials (e.g., biased ferrimagnetic materials with a gyrotropic *permittivity* tensor) exhibit very weak nonreciprocal properties [22], implying that large bias fields, or long propagation lengths (from tens to thousands of wavelengths), or narrow-band resonant structures, are required to achieve significant isolation [23, 24].

Motivated by these outstanding challenges, in this Letter we propose a new approach to enhance broadband nonreciprocal effects in compact plasmonic structures. We revisit the dispersion characteristics of the permittivity model of a standard magnetized plasmonic material and unveil a previously overlooked regime of broadband and giant nonreciprocity below the cyclotron resonance frequency. This enables the realization of broadband isolators operating over more than a decade with low insertion loss and ultra-compact footprint, at the scale of the wavelength or smaller.

We consider the simplest model of a nonreciprocal plasmonic medium, namely, a magnetized Drude plasma. For nonzero static magnetic bias, such a medium is anisotropic and gyrotropic, and its electromagnetic response is represented by a frequency-dispersive, asymmetric permittivity tensor  $\bar{\epsilon}$ . For propagation along the direction of the bias (Faraday configuration), a diagonalization of  $\bar{\epsilon}$  shows that each circularly polarized (CP) eigenmode experiences a different effective permittivity  $\epsilon_{\pm}$  (right-handed CP denoted by “−” and left-handed CP by “+”). This creates a nonreciprocal phase

shift between left-handed and right-handed CP waves if they are both allowed to propagate; therefore, a linearly polarized propagating wave experiences a polarization-plane rotation of  $\Delta\Phi$  (Faraday rotation angle). To realize an isolator, it is then necessary to implement  $\Delta\Phi = \pi/4$ , such that a reflected wave undergoes a  $\pi/2$  polarization rotation over a roundtrip, and insert a polarizer to filter out the rotated field at the input port.

The effective relative permittivity seen by the CP modes and the Faraday rotation angle (assuming free-space permeability) are given by (Ch. III.20 in Ref. [1])

$$\varepsilon_{\pm}(\omega) = \varepsilon_{\infty} \left[ 1 - \frac{\omega_p^2}{\omega(\omega \pm \omega_c + i\gamma)} \right], \quad (1)$$

$$\Delta\Phi(\omega) = \frac{L}{2c_0} \omega \left( \Re[\sqrt{\varepsilon_-(\omega)}] - \Re[\sqrt{\varepsilon_+(\omega)}] \right), \quad (2)$$

where  $\omega_p$  is the plasma frequency,  $\omega_c = eB_0/m^*$  is the cyclotron frequency, with  $B_0$  being the magnitude of the static bias field and  $m^*$  the electron effective mass,  $e$  is the electron charge,  $\varepsilon_{\infty}$  is the permittivity at high frequencies (bound-charge contribution),  $\gamma$  is the loss coefficient,  $L$  is the length of the medium, and  $c_0$  is the free-space light speed. Throughout the paper, we assume a  $e^{-i\omega t}$  time-harmonic dependence for all fields. As shown in Fig. 1,  $\varepsilon_-$  (RCP mode) exhibits a resonance at  $\omega_c$ , corresponding to the frequency of the cyclotron motion of the plasma electrons under a static magnetic bias; this mode is denoted as the extraordinary mode. On the contrary, for the LCP mode, the material behaves as an ordinary Drude-like plasma, i.e.,  $\varepsilon_+$  increases monotonically with frequency, albeit with a shifted plasma frequency. Frequencies at which  $\varepsilon_{\pm}$  crosses zero mark the limits of the propagation regions of interest, and are given by  $\omega_{\pm} = \sqrt{\omega_p^2 + \omega_c^2/4} \mp \omega_c/2$ .

In order to gain more physical insight into the dispersion characteristics of this permittivity model, it is crucial to appreciate how the principle of causality implies certain conditions and constraints, expressed through Kramers-Kronig (K-K) relations, which relate the real  $\Re$  and imaginary  $\Im$  parts of the permittivity function. Notably, using K-K relations, it is expected that  $\partial\Re[\varepsilon(\omega)]/\partial\omega > 0$  for passive materials in low-loss frequency windows (see Eq. (84.1) in Ref. [25], and the Appendix). However, as seen in Fig. 1(a), while this condition applies to the LCP mode permittivity at all frequencies, it fails to describe the behaviour of the RCP mode permittivity in the low-loss region below resonance. Therefore, this may raise concerns about the applicability of K-K relations to gyrotropic plasmonic materials and, consequently, about the implications of causality for these media. In addition, we note that, for a non-zero cyclotron frequency (non-zero bias), the so-called ‘‘reality condition’’ (which implies a real time-domain response) is also violated in these materials:  $\Re[\varepsilon_{\pm}(\omega)] \neq \Re[\varepsilon_{\pm}(-\omega)]$  and  $\Im[\varepsilon_{\pm}(\omega)] \neq -\Im[\varepsilon_{\pm}(-\omega)]$ .

While these apparent issues may seem surprising, we argue that they simply originate from the fact that  $\varepsilon_{\pm}$  are not elements of the permittivity tensor  $\bar{\varepsilon}$ , but eigenvalues that are

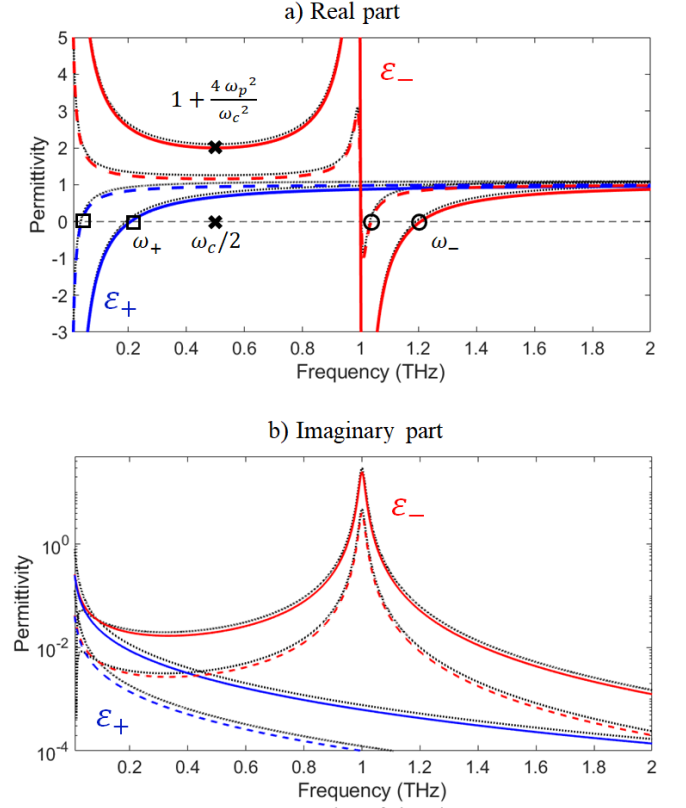


FIG. 1. Real part (a) and imaginary part (b) of the effective scalar permittivity for RCP ( $\varepsilon_-$ ) and LCP ( $\varepsilon_+$ ) modes, with  $\omega_c/2\pi = 1$  THz,  $\gamma = 0.01\omega_c$ ,  $\omega_c/\omega_p = 2$  (5) for solid (dashed) lines, assuming  $\varepsilon_{\infty} = 1$ . The dotted black lines represent the permittivity values derived using the modified Kramers-Kronig relations, shifted slightly upwards for clarity. The two regions of interest (in which both modes propagate with low loss) are: (i) the transparent region above  $\omega_-$  (small circle), and (ii) the transparent window, opened by the static bias, extending from  $\omega_+$  (small square) to  $\omega_c/2$  (cross). The region below  $\omega_+$  is not of interest because the ordinary mode is an evanescent wave (negative permittivity); therefore, Faraday rotation is not possible.

combinations of diagonal and non-diagonal elements. Therefore, the inverse Fourier transform of  $\varepsilon_{\pm}$  does not represent a ‘‘true’’ time-domain response function, and is not expected to be real. Nevertheless, this fact does not prohibit the derivation of K-K relations, since the functions  $\varepsilon_{\pm}$  inherit the analyticity of the tensor elements (no poles in the upper half of the complex frequency plane). However, to obtain the correct K-K relations for  $\varepsilon_{\pm}$ , it is crucial to properly take into account the contribution of the pole at  $\omega = 0$  on the real frequency axis, which leads to an additional term for the K-K relation of the real part of the permittivity, compared to the standard K-K relation:

$$\Re[\varepsilon_{\pm}(\omega)] = 1 + \frac{1}{\pi} \int_{-\infty}^{\infty} d\Omega \frac{\Im[\varepsilon_{\pm}(\Omega)]}{(\Omega - \omega)} \mp \frac{\omega_p^2 \omega_c}{\omega(\omega_c^2 + \gamma^2)}, \quad (3)$$

Further details on the modified K-K relations and their de-

tailed derivation are available in the Appendix.

The results in Fig. 1 show that the permittivity functions (dotted black lines) derived from the modified K-K relations, Eqs. (3) and (7), exactly match the analytical permittivity expressions (1) for both the real and imaginary parts, which confirms the causality of the standard permittivity model of a magnetized plasma. Most importantly, however, due to the aforementioned additional term in the K-K relation (3), the positive dispersion constraint,  $\partial \Re[\varepsilon(\omega)]/\partial \omega > 0$  in low-loss windows, is no longer guaranteed, as demonstrated by the extraordinary mode permittivity. In other words, anomalous (negative) dispersion is possible in this passive material, even in low-loss regions far from resonance. This makes the dispersion characteristics of a gyrotropic plasma fundamentally richer (non-monotonic) than any isotropic materials. As discussed next, this non-monotonic behavior can provide, under certain conditions, a natural form of dispersion compensation, and lays the foundations for achieving broadband giant non-reciprocity in magnetized plasmonic devices.

In order to achieve broadband Faraday rotation, with  $\Delta\Phi(\omega)$  approximately constant as a function of frequency, we need  $(\Re[\sqrt{\varepsilon_-(\omega)}] - \Re[\sqrt{\varepsilon_+(\omega)}]) \propto \omega^{-1}$  over an extended frequency region, as deduced from Eq. (2). Two candidate regions can be identified in Fig. 1(a), where both permittivity functions are positive (propagating waves) and approach each other as frequency increases. The first region of interest is the transparent region above  $\omega_-$ , which is the most widely studied regime for Faraday rotation in plasmonic materials [1, 26–28]. In this region, the permittivity function of both modes,  $\varepsilon_{\pm}$ , monotonically increases with frequency and it approaches unity from below for  $\omega \rightarrow \infty$ . Therefore, the Faraday rotation angle at high frequencies, where  $\omega \gg \omega_p, \omega_c, \gamma$ , is approximately given by  $\Delta\Phi \propto \omega^{-2}$ , as indicated in Fig. 2(a) (this is the region conventionally associated with the definition of Verdet constant [1]). Thus, in this regime, the material does not exhibit a broadband, dispersion-less, nonreciprocal behavior (conversely, due to their different microscopic material response, biased ferrites show non-dispersive behavior in a similar “far-from-resonance” region, see, e.g., Eq. (7-18) in Ref. [2]).

The other region of interest, which has been overlooked so far in the literature, is below the cyclotron resonance, and is defined as the frequency range  $\omega_+ \leq \omega \leq \omega_c/2$ , provided that the cyclotron frequency is sufficiently high,  $\omega_c > 2\omega_p/\sqrt{3}$ , which assures the region existence as  $\omega_c/2 > \omega_+$ . This corresponds to the anomalous-dispersion window in which  $\partial \Re[\varepsilon(\omega)]/\partial \omega < 0$  for the extraordinary mode. Note that, for any nonzero value of plasma frequency,  $\omega_p \neq 0$ , the extraordinary (ordinary) mode permittivity below resonance is always larger (smaller) than unity (or, more generally, the constant  $\varepsilon_{\infty}$ ) as seen in Fig. 1(a). In the limit  $\omega_c \gg \omega_p$ , both permittivities,  $\varepsilon_{\pm}$ , approach unity (or  $\varepsilon_{\infty}$ ) from opposite sides in this frequency window. Consequently, using a Taylor expansion, one arrives at  $(\Re[\sqrt{\varepsilon_-(\omega)}] - \Re[\sqrt{\varepsilon_+(\omega)}]) \approx (\sqrt{\varepsilon_{\infty}} \omega_p^2/\omega_c) \omega^{-1}$ . As discussed above, this is the de-

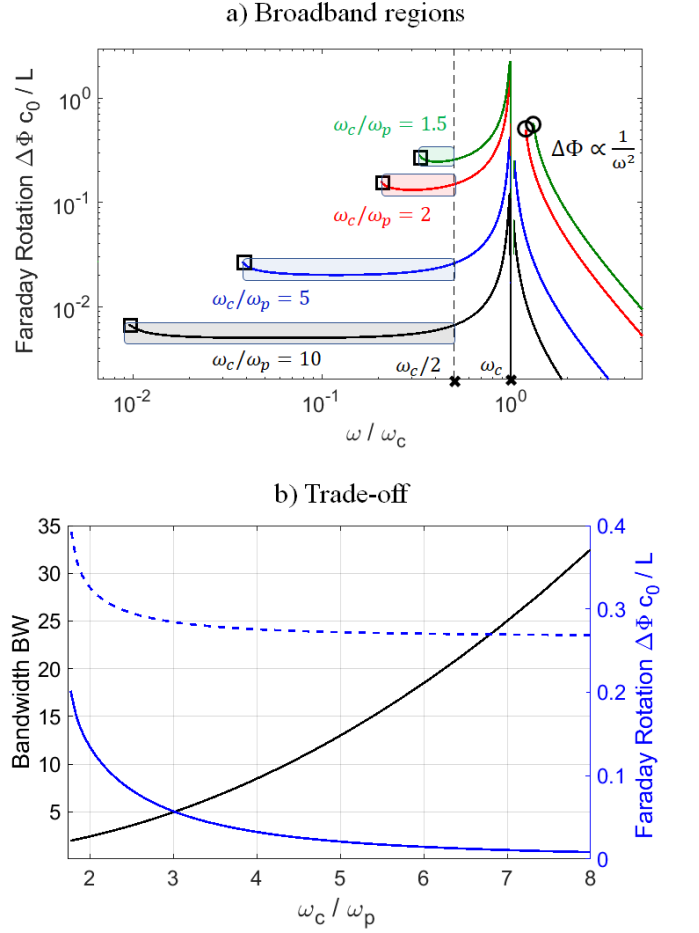


FIG. 2. (a) Broadband regions of Faraday rotation (shaded areas) below the resonance frequency, with  $\omega_c > 2\omega_p/\sqrt{3}$ , as discussed in the text. The different curves show the normalized Faraday rotation angle,  $\Delta\Phi c_0/L$ , for different values of  $\omega_c/\omega_p$ . We set  $\varepsilon_{\infty} = 1$  and  $\gamma = 0.01$ . (b) A fundamental trade-off appears between the width of the broadband region and the achievable Faraday rotation angle for different values of  $\omega_c/\omega_p$ . The width BW of the broadband region is defined here as the ratio  $(\omega_c/2)/(\omega_+)$ . The dashed line represents the *rotation-bandwidth product*, as defined in the text.

sired frequency dependence to achieve broadband response: consistent with Eq. (2), Faraday rotation is approximately dispersion-less in this region. The broadband behavior is demonstrated in Fig. 2(a), where it is clear that the Faraday rotation angle gets less frequency dispersive as  $\omega_c/\omega_p$  increases. We would like to stress, however, that broadband Faraday rotation with low dispersion can still be obtained even if  $\omega_c$  and  $\omega_p$  are comparable. For example, for an octave- (or a decade-) wide broadband region, it is required that  $\omega_c/\omega_p > 1.8$  (or 4.4), as shown in Fig. 2(b).

Attaining comparable cyclotron and plasma frequency such that  $\omega_c > 2\omega_p/\sqrt{3}$  may seem challenging (and it usually is) since it typically requires large magnetic bias. This issue may be circumvented using a metamaterial approach to lower  $\omega_p$  [29]. Alternatively,  $\omega_c > \omega_p$  is feasible in certain solid-state plasmas with small effective electron mass, as the

ratio  $\omega_c/\omega_p$  is proportional to  $1/\sqrt{m^*}$ . This has been experimentally demonstrated in, for example, *n*-doped Indium Antimonide (InSb) under moderate bias at THz frequencies [30–32].

An interesting trade-off appears in Fig. 2 between the achievable Faraday rotation angle and the width of the broadband region. As  $\omega_c/\omega_p$  increases, the difference between the permittivity values seen by RCP and LCP modes decreases, as shown in Fig. 1(a) (compare the solid and dashed lines), which implies a smaller Faraday rotation angle. This can be quantified as follows: let the system length  $L$  be defined in terms of the center wavelength of the considered band, that is,  $L = a\lambda_s$ , where  $a$  is the normalized length, and  $\omega_s = 2\pi c_0/\lambda_s$ . Then, by letting  $\omega_s = \omega_c/4$ , the Faraday rotation angle can be approximately written as  $\Delta\Phi \approx 4.3\pi a\sqrt{\varepsilon_\infty}\omega_p^2/\omega_c^2$ . At the same time, increasing  $\omega_c/\omega_p$  leads to a decrease of the lower-frequency limit,  $\omega_+$ , of the broadband region, hence further broadening it. The bandwidth of the dispersion-less window in the  $\omega_c \gg \omega_p$  limit can then be approximated as  $BW \approx 0.5\omega_c^2/\omega_p^2$  (bandwidth defined as the ratio of high-frequency and the low-frequency limits, as in Fig. 2). Thus, under the assumption of large  $\omega_c/\omega_p$ , we can define an approximate *rotation-bandwidth product*,

$$BW \times \Delta\Phi \approx 2.15\pi a\sqrt{\varepsilon_\infty}, \quad (4)$$

which quantifies the trade-off between maximum rotation and maximum bandwidth, with the bound uniquely determined by the length of the device and the high-frequency permittivity. This trade-off can be used as a metric for design optimization for broadband nonreciprocal devices operating in this new regime. We stress that, even with the limitations expressed by the rotation-bandwidth product, the Faraday rotation angles achievable in this below-resonance broadband region are significantly larger than their counterpart in the far-from-resonance high-frequency region, as can be seen in Fig. 2(a). This enables the realization of not only broadband but also ultra-compact nonreciprocal components.

As a rather striking example of broadband giant nonreciprocity in this new regime, we present designs for a deeply subwavelength broadband Faraday isolator operating at THz frequencies at room temperature (which is the first of its kind to our knowledge). As mentioned earlier, we choose *n*-type InSb due to its unparalleled potential for nonreciprocal devices at THz frequencies [31], thanks to its low effective mass, high electron mobility, relatively low losses, and large  $\varepsilon_\infty \approx 15.68$  [33]. The temperature dependence of  $\omega_p(T)$ , loss coefficient  $\gamma(\omega)$ , and other parameters of InSb are adopted from Ref. [34].

To design a broadband and efficient isolator, our goal is to achieve  $\Delta\Phi = \pi/4$  within a  $\pm 2.5\%$  margin (chosen arbitrarily) over the operational band, with power transmission above 85% (insertion loss below 0.7 dB), by optimizing the magnetic bias  $B_0$  and the plasma frequency, while keeping the length  $L$  of the device as small as possible. If the bias is fixed, the factor that primarily determines the bandwidth

is the plasma frequency, which can be controlled through the temperature or doping.

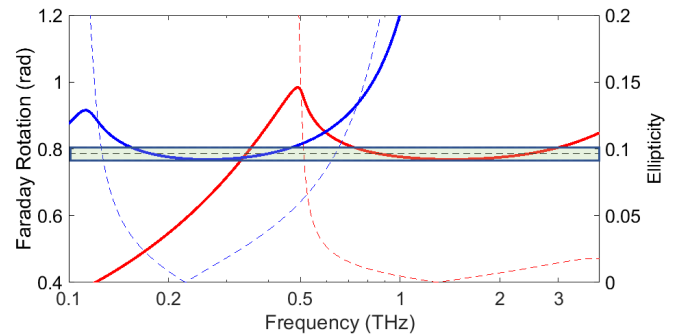


FIG. 3. Two examples of subwavelength broadband Faraday rotator at THz frequencies using *n*-type InSb: (red solid) moderately strong bias,  $B_0 = 5$  T, at room temperature, 290 K; and (blue solid) sub-Tesla bias,  $B_0 = 0.77$  T, at 170 K. The rotation angle remains around  $\pi/4$  (shaded area) across the operational band. Dashed lines represent the ellipticity for each case (the smaller the better). The other parameters are given in the text.

As an example, the red curve in Fig. 3 is for a subwavelength slab of InSb with  $L = 33 \mu\text{m}$  ( $a = 0.192$ ),  $B_0 = 5$  T, at room temperature  $T = 290$  K. By using a suitable polarizer, this subwavelength structure can then work as a broadband and efficient isolator that covers the 0.7 – 3 THz band. To cover the lower frequencies in the high-GHz regime, a lower plasma frequency is required, which can be obtained by reducing the doping or the temperature. The blue curve in Fig. 3 is for another subwavelength Faraday rotator with  $L = 0.138$  mm ( $a = 0.15$ ), and a much lower bias,  $B_0 = 0.77$  T, at  $T = 170$  K, which covers the band 0.15–0.45 THz. Both cases in Fig. 3 exhibit the required Faraday rotation within the specified margin of  $\pm 2.5\%$  and with transmitted power above 85% (due to the presence of unavoidable losses in the plasmonic material), assuming matched isolator ports using suitable anti-reflection coatings. For completeness, in Fig. 3, we also characterize the isolator dichroism (polarization-dependent absorption) based on the ellipticity parameter, which is typically defined as the difference between the amplitudes of the two propagating CP waves divided by their sum. Ellipticity needs to be minimized to ensure that the linearly-polarized state of the wave is preserved as it propagates through the Faraday isolator, so that a reflected wave is efficiently absorbed by the polarizer. As shown in Fig. 3, the ellipticity is negligible for both cases across the indicated operational bands.

In conclusion, by revisiting the dispersion properties of gyrotropic plasmonic materials and having clarified the implications of causality in this case, we have unveiled a previously overlooked regime of wave propagation in biased plasmas, characterized by anomalous dispersion and low losses. This leads to a broadband window of dispersion-less Faraday rotation, which could extend over more than a decade-wide frequency band. Contrary to the conventional regime of

operation of magnetized plasmas and ferrites, this broadband window is closer to resonance and, therefore, is characterized by stronger nonreciprocity, hence enabling the realization of deeply subwavelength nonreciprocal devices ( $a \ll 1$ ), with an orders-of-magnitude reduction in length for the same level of bias intensity.

The approach and results presented in this Letter may pave the way toward superior nonreciprocal components that can be optimized for both broadband operation and compactness. We expect our findings to be particularly appealing for various emerging applications within the wide ‘‘THz gap,’’ where efficient nonreciprocal devices based on biased ferrites or spatiotemporally modulated structures are difficult to realize.

#### APPENDIX: Kramers-Kronig relations for gyrotropic plasmonic media

Certain physical constraints exist that restrict the response function of any physical system, regardless of its specific details. For instance, causality ensures the analyticity of the permittivity function  $\varepsilon(\omega)$  in the upper half of the complex frequency plane. Using the residue theorem, this property leads to the following relation:

$$\oint_{\Gamma} d\Omega \frac{\varepsilon(\Omega) - 1}{\Omega - \omega} = 0, \quad (5)$$

where  $\Gamma$  is an arbitrarily closed contour in the upper half plane. For the plasma model used in this letter,  $\varepsilon(\omega)$  has a pole on the real axis at  $\omega = 0$ . Thus, let  $\varepsilon(\omega) - 1 = \chi(\omega) = \chi_0(\omega)/\omega$ , where  $\chi_0(\omega)$  is analytic in the upper half plane and on the entire real axis. Now let the closed integration path  $\Gamma$  be an infinite semicircle in the upper half plane, excluding the poles at  $\Omega = 0$  and  $\Omega = \omega$ , i.e.,  $\Gamma = I_{\infty} + I_R + I_{C1} + I_{C2}$ , as shown in Fig. 4. For such a causal system, and given that the energy of any physical interaction is necessarily finite, it can always be ensured through Titchmarsh theorem that  $[\chi_0(\omega)] \rightarrow 0$  as  $|\omega| \rightarrow \infty$  [35]. In this case, the integral over the semi-infinite circle  $I_{\infty}$  evaluates to zero.

Then, by evaluating the two infinitesimal semicircles  $I_{C1}$  and  $I_{C2}$  around the poles, Eq. (5) becomes

$$\int_{-\infty}^{\infty} d\Omega \frac{\chi_0(\Omega)}{\Omega(\Omega - \omega)} + i\pi \frac{\chi_0(0)}{\omega} - i\pi \frac{\chi_0(\omega)}{\omega} = 0, \quad (6)$$

where the integral  $\int$  is the Cauchy Principle-Value integral defined over  $\mathbb{R} - \{0, \omega\}$ , represented by  $I_R$ . Crucially,  $\omega \neq 0$  is required, otherwise, the integrand would have a second-order pole at  $\Omega = 0$ , and such a PV integral diverges for second-order poles. It is also important to stress that  $\int d\Omega/\Omega$  must be approached symmetrically to be correctly defined (and so that it converges) [36].

By rearranging, we arrive at the modified K-K relations for magnetized plasmonic materials valid for both  $\varepsilon_{\pm}$  (for  $\omega \neq 0$ ),

$$\Re[\varepsilon(\omega)] = 1 + \frac{1}{\pi} \int_{-\infty}^{\infty} d\Omega \frac{\Im[\varepsilon(\Omega)]}{(\Omega - \omega)} + \frac{\Re[\chi_0(0)]}{\omega}, \quad (7a)$$

$$\Im[\varepsilon(\omega)] = \frac{-1}{\pi} \int_{-\infty}^{\infty} d\Omega \frac{\Re[\varepsilon(\Omega) - 1]}{(\Omega - \omega)} + \frac{\Im[\chi_0(0)]}{\omega}. \quad (7b)$$

For the case of a non-magnetized plasma described by a scalar lossy Drude model,  $\Re[\chi_0(0)] = 0$ , and since  $\Im[\varepsilon(\Omega)]$  is positive at all frequencies in passive media, it is straightforward to show that the frequency derivative of the real part of the permittivity (7a) is always positive in low-loss frequency windows [25], corresponding to normal dispersion. This is not valid in the case of gyrotropic plasmas because  $\Re[\chi_0(0)] = \mp \omega_p^2 \omega_c / (\omega_c^2 + \gamma^2) \neq 0$ ; therefore, it is easy to see that, for the extraordinary mode, the normal-dispersion constraint  $\partial \Re[\varepsilon(\omega)] / \partial \omega > 0$  can no longer be assumed to be valid in low-loss windows. In particular, in any low-loss region, we get

$$\frac{\partial \Re[\varepsilon_{\pm}(\omega)]}{\partial \omega} = \frac{1}{\pi} \int_{-\infty}^{\infty} d\Omega \frac{\Im[\varepsilon(\Omega)]}{(\Omega - \omega)^2} - \frac{\Re[\chi_0(0)]}{\omega^2}, \quad (8)$$

from which it is clear that the negative term is dominant at low frequencies for the extraordinary mode (corresponding to the anomalous dispersion region discussed in the main text).

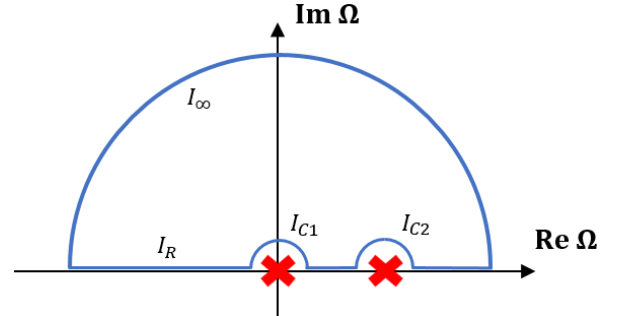


FIG. 4. The integral path  $\Gamma$  in the complex frequency plane used to derive the modified Kramers-Kronig relations for the effective permittivity of gyrotropic plasmas.

\* mia37@cornell.edu

† francesco.monticone@cornell.edu

- [1] A. Sommerfeld, *Lectures on theoretical physics: Optics*, Vol. 4 (Academic press, 1954).
- [2] B. Lax and K. J. Button, *Microwave ferrites and ferrimagnetics* (McGraw-Hill, 1962).
- [3] D. M. Pozar, *Microwave engineering* (John Wiley & Sons, 2009).
- [4] Z. Yu and S. Fan, *Nature Photonics* **3**, 91 (2009).
- [5] D. L. Sounas, C. Caloz, and A. Alu, *Nature Communications* **4**, 1 (2013).
- [6] Y. E. Wang, in *2012 IEEE International Conference on Wireless Information Technology and Systems (ICWITS)* (2012) pp. 1–4.

- [7] C. Caloz and Z.-L. Deck-Léger, *IEEE Transactions on Antennas and Propagation* **68**, 1569 (2019).
- [8] D. L. Sounas and A. Alù, *Nature Photonics* **11**, 774 (2017).
- [9] K. Gallo, G. Assanto, K. R. Parameswaran, and M. M. Fejer, *Applied Physics Letters* **79**, 314 (2001).
- [10] L. Fan, J. Wang, L. T. Varghese, H. Shen, B. Niu, Y. Xuan, A. M. Weiner, and M. Qi, *Science* **335**, 447 (2012).
- [11] Y. Shi, Z. Yu, and S. Fan, *Nature Photonics* **9**, 388 (2015).
- [12] C. Caloz, A. Alù, S. Tretyakov, D. Sounas, K. Achouri, and Z.-L. Deck-Léger, *Physical Review Applied* **10**, 047001 (2018).
- [13] A. Y. Pawar, D. D. Sonawane, K. B. Erande, and D. V. Derle, *Drug invention today* **5**, 157 (2013).
- [14] W. L. Chan, J. Deibel, and D. M. Mittleman, *Reports on progress in physics* **70**, 1325 (2007).
- [15] R. Piesiewicz, T. Kleine-Ostmann, N. Krumbholz, D. Mittleman, M. Koch, J. Schoebei, and T. Kurner, *IEEE Antennas and Propagation Magazine* **49**, 24 (2007).
- [16] D. Mittleman, *Sensing with terahertz radiation*, Vol. 85 (Springer, 2013).
- [17] P. Schulz, *Applied Optics* **28**, 4458 (1989).
- [18] E. S. Dimova, D. Comparat, G. S. Popkirov, A. Rangelov, and N. Vitanov, *Applied Optics* **52**, 8528 (2013).
- [19] D. L. Sounas, J. Soric, and A. Alu, *Nature Electronics* **1**, 113 (2018).
- [20] T. Dinc, M. Tymchenko, A. Nagulu, D. Sounas, A. Alu, and H. Krishnaswamy, *Nature Communications* **8**, 1 (2017).
- [21] M. Shalaby, M. Peccianti, Y. Ozturk, and R. Morandotti, *Nature Communications* **4**, 1 (2013).
- [22] A. K. Zvezdin and V. A. Kotov, *Modern magneto-optics and magneto-optical materials* (CRC Press, 1997).
- [23] Q. Du, C. Wang, Y. Zhang, Y. Zhang, T. Fakhrul, W. Zhang, C. Goncalves, C. Blanco, K. Richardson, L. Deng, *et al.*, *ACS Photonics* **5**, 5010 (2018).
- [24] Y. Zhang, Q. Du, C. Wang, T. Fakhrul, S. Liu, L. Deng, D. Huang, P. Pintus, J. Bowers, C. A. Ross, *et al.*, *Optica* **6**, 473 (2019).
- [25] L. D. Landau, J. Bell, M. Kearsley, L. Pitaevskii, E. Lifshitz, and J. Sykes, *Electrodynamics of continuous media*, Vol. 8 (elsevier, 2013).
- [26] L. Aplet and J. Carson, *Applied Optics* **3**, 544 (1964).
- [27] L. Weller, K. Kleinbach, M. A. Zentile, S. Knappe, I. Hughes, and C. Adams, *Optics Letters* **37**, 3405 (2012).
- [28] B. J. Stadler and T. Mizumoto, *IEEE Photonics Journal* **6**, 1 (2013).
- [29] J. B. Pendry, A. Holden, W. Stewart, and I. Youngs, *Physical Review Letters* **76**, 4773 (1996).
- [30] X. Wang, A. Belyanin, S. Crooker, D. Mittleman, and J. Kono, *Nature Physics* **6**, 126 (2010).
- [31] T. Arikawa, X. Wang, A. A. Belyanin, and J. Kono, *Optics Express* **20**, 19484 (2012).
- [32] D. Wang, B. Yang, W. Gao, H. Jia, Q. Yang, X. Chen, M. Wei, C. Liu, M. Navarro-Cía, J. Han, *et al.*, *Nature Physics* **15**, 1150 (2019).
- [33] The InSb permittivity model at THz frequencies includes an additional resonance term due to phonon contribution at 5.9 THz. We limit our investigation to frequencies below this resonance to avoid an additional source of losses.
- [34] Q. Mu, F. Fan, S. Chen, S. Xu, C. Xiong, X. Zhang, X. Wang, and S. Chang, *Photonics Research* **7**, 325 (2019).
- [35] H. Fearn, *Journal of Modern Optics* **53**, 2569 (2006).
- [36] G. B. Arfken and H. J. Weber, *Mathematical methods for physicists* (American Association of Physics Teachers, 1999).